The Visual System of the Blind Shark (*Brachaelurus waddi*)

Olivia Seeger

Department of Biological Sciences

Macquarie University

olivia.seeger@hdr.mq.edu.au

This thesis is presented for the degree of Master of Research

November 9th, 2018

This thesis is formatted for the Journal of Experimental Biology

Declaration

I wish to acknowledge the following assistance in the research detailed in this report:

Supervisors: Associate Professor Nathan Hart and Dr. Laura Ryan for guiding my experimental design and analysis.

Ethics Approval: All research performed on animals was approved by Macquarie University's Animal Ethics Committee, Animal Research Authority 2017/039 and Scientific NSW Department of Primary Industries and Fisheries scientific collection permit P17/0055-1.0

All other research described in this report is my own original work.

Olivia S. Seeger

November 9th, 2018

Acknowledgements

First and foremost, I would like to thank my primary supervisor Associate Professor Nathan Hart. His academic advice and mentoring over these past two years has enabled me to grow tremendously as an independent researcher.

Second, I would like to thank my co-supervisor, mentor, and friend Dr. Laura Ryan. She has gone above and beyond as a supervisor and mentor and I can't thank her enough for taking the plunge and taking me on as her first student. The countless hours and weekends she gave up to teach me these past two years have not gone unnoticed.

Next, I would like to recognize Dr. Yuri Ogawa who played a part in teaching me the fundamentals of electrophysiology and making me realize ants are way less stressful to study than sharks. My thanks also to the remainder of the neurobiology lab for their constant support.

I also want to acknowledge Tristan Guillemin who was always so enthusiastic to go fishing with me. He is an excellent teacher and taught me everything I needed to know about fishing.

As an international student, this journey has been especially tough, but I want to acknowledge and thank my family who have done nothing but shower me with support. Since I moved from Greensboro, North Carolina (USA) to embark on this journey 3,000 miles away in Sydney Australia, my family's constant and unwavering love is what got me through it in the end. Thank you, especially to my parents, who taught me anything worth having is worth fighting for and may they always remember who the lucky one really is.

Thank you to all of my friends, especially Nickolas Singh and Lou Tosetto, who have been huge pillars for me to lean on in the everyday stresses of completing a thesis. From proofreading to lunches and dinners, both have been there for me during the highs and lows of what has been a rollercoaster of a year.

Table of Contents

Abstract

Sharks have evolved over a period of approximately 400 million years. This extensive timeframe has resulted in a divergence of shark species that occupy a wide range of environments and exhibit considerable diversity in morphology and behavior. It is likely that this diversity is reflected in the anatomy and physiology of shark visual systems. However, only a very small proportion of extant shark species has been studied in detail and much remains to be discovered about interspecific variation in their visual system. Furthermore, there have been no studies to date that have undertaken a comprehensive assessment of the visual abilities of a single shark species. Blind sharks (*Brachaelurus waddi*) are a benthic species found in abundance along Australia's coast and adapt well in captivity, which makes them amenable to an in-depth assessment of their visual system. In this study, the anatomy and physiology of the blind shark's eye was investigated and the results interpreted within the context of their environment and behavior. Electrophysiological techniques were used to measure the temporal resolution and contrast sensitivity of the eye. The spectral absorption properties of the photoreceptor visual pigments that subserve vision were measured in situ using single cell microspectrophotometry. Spatial resolving power was assessed by measuring the topographic distribution of ganglion cells in wholemounted retinas. When presented with a sinusoidally modulated light stimulus, blind sharks have a maximum critical flicker fusion rate of 22 Hz and a contrast sensitivity threshold of 177.6 (0.56%) at the brightest light intensity. Rods were the only type of photoreceptor identified in the retina. The rods contained a medium-wavelength ('green') sensitive visual pigment with a mean λ_{max} at 501 nm. The topographic distribution of ganglion cells in *B. waddi* showed a weakly defined, elongated horizontal band or visual streak of higher density in the central-dorsal region of the retina. Based on the mean peak density of ganglion cells in the retina, the estimated spatial resolving power of the eye was 2.36 cycles per degree (cpd).

1. INTRODUCTION

Over the course of approximately 500 million years, the vertebrate eye has evolved from a basic light processing organ into a complex neurological system (Land and Nilsson, 2012). Visual processing provides animals with information about the environment (Coren and Girgus, 1978). The visual system of a particular species may be specialized to detect certain image characteristics over others, such as the overall size of an object as opposed to fine details (Duncan, 1984). This is due to the multiple physiological and anatomical adaptations of the visual system to suit the various behavioral needs and environmental constraints of animals (Walls, 1942, Collin and Pettigrew, 1988, Hueter, 1991, Lisney et al., 2012). For example, rod photoreceptors respond at a slower rate than cone photoreceptors but work best in dim light environments, whereas cone photoreceptors respond at a faster rate and operate better in bright light. Accordingly, nocturnal species typically have relatively higher densities of rod photoreceptors as opposed to diurnal species that show relatively larger densities of cone photoreceptors (Lisney et al., 2012). Such adaptations have been critical in meeting the visual demands of an animal's environment, influencing its ability to capture prey, avoid predators, communicate and navigate (Walls, 1942, Warrant and Locket, 2004, Kelley and Kelley, 2014).

The visual demands in aquatic environments are considerably different to those in terrestrial habitats (Warrant and Locket, 2004, Hart et al., 2006, Malmstrom and Kroger, 2006). The aquatic environment has particular challenges due to the physical properties of water (McFarland, 1986). Light attenuation is particularly significant in the aquatic environment due to reflection, absorption and scatter by water itself and other dissolved or suspended substances (Gramoni and Ali, 1970, McFarland, 1990, Flamarique and Hawryshyn, 1997); consequently, light intensity is substantially reduced as depth increases (Gramoni and Ali, 1970). To deal with the low light levels in the aquatic environment the retina of aquatic species that are deep-dwelling or nocturnal typically have larger photoreceptor outer segments and/or longer integration times to improve photon capture and thus sensitivity (McFarland and Loew, 1883, Conner and MacLeod, 1977).

Similarly, the spectral distribution of light is also affected in aquatic environments. Water absorbs longer (redder) wavelengths of light more readily than shorter (bluer) wavelengths. This explains why blue light is dominant in clear oceanic water (Warrant and Johnsen, 2013). Coastal marine

waters and freshwater with a high content of chlorophyll and other dissolved organic substances have different wavelength absorption profiles, typically resulting in greener water colors (Land and Nilsson, 2012, Warrant and Johnsen, 2013). Previous studies have shown that the visual pigments in the retinal photoreceptors of fishes are generally tuned to match the spectrum of light within a species' habitat (Clarke 1936). For example, the visual pigments of marine species, especially those occupying coral reefs, tend to have wavelengths of peak absorbance (λ_{max}) at shorter wavelengths, whereas species inhabiting coastal marine habitats have visual pigments with λ_{max} values at longer wavelengths, and fish in turbid or colored freshwater lakes and rivers tend to have pigments with λ_{max} at the longest wavelengths (Loew and Lythgoe, 1978, Lythgoe, 1980, Hart et al., 2006).

These observed correlations presumably reflect ecological demands in the aquatic eye. However, many visual adaptations come at a cost to other visual adaptions such that an animal's eye 'design' presumably reflects a number of structural and functional trade-offs. A rod-dominated retina can impact an animal's ability to perform certain visual tasks, such as resolving fast moving objects, because rod photoreceptors respond more slowly to changing light intensities than cones (Dowling and Ripps, 1970). Temporal resolution measures the eye's ability to resolve moving images (Gramoni and Ali, 1970). Low temporal resolution may result in the object appearing as a motion-blurred image (Warrant, 1999, Fritsches et al., 2005, Cohen and Frank, 2006). Animals that have fast moving prey or predators or occupy shallow waters typically have a higher temporal resolution (>30 Hz) (Warrant, 1999, Kalinoski et al., 2014, Warrington et al., 2017). Moreover, deep water inhabitants typically have lower temporal resolution (i.e. longer integration time) which improves photon capture (Lisney et al., 2012). However, longer integration times potentially improve an animal's absolute and contrast sensitivity (Asi and Perlman, 1992, Cao et al., 2007) i.e. a higher contrast sensitivity improves an animal's ability to distinguish objects against a similar background (Wandell, 1996). In dimly lit aquatic environments contrast is low and animals may rely on high contrast sensitivity to meet their visual demands. Therefore, in the aquatic environment high spatial resolution may not be favored, but high contrast sensitivity may be a greater visual advantage (Warrant, 1999). Understanding the visual capabilities of an animal provides insight to its behavioral and environmental adaptations.

Sharks have evolved over approximately 400 million years (McComb et al., 2010) and have diverged into approximately 500 different species occupying a range of habitats across freshwater and coastal environments (Ebert et al., 2013). This makes sharks a fascinating taxon to study and based on limited data it would appear that the shark eye has evolved to reflect behavior and environment, presumably to improve visual performance for different tasks and conditions (Hart et al., 2006, Lisney et al., 2012). Having a greater understanding of shark visual systems will provide further insight into evolutionary pressures on vertebrate eye design.

Sharks rely heavily on vision for survival; however, little is known about the fundamental capabilities of their visual system (Lisney et al., 2012). Only a small number of studies have focused on eye morphology and spectral sensitivity in sharks, and even fewer have measured the temporal resolution and contrast sensitivity capabilities of the eye (McComb et al., 2010, Hart et al., 2011, Schieber et al., 2012, Ryan et al., 2017). Common with most vertebrates, the morphology of the shark's retina shows areas of specialization with higher cell densities to increase the spatial resolving power of the eye (Hughes, 1971). These areas are sometimes seen in the form of a band, or visual streak, across a shark's retina. Visual streaks potentially help improve tasks such as scanning for prey over a large area with minimal eye movement (Collin and Pettigrew, 1988). Some species have evolved low rod-to-cone ratios that can improve visual performance when detecting fast moving objects or high rod-to-cone ratios to improve photon capture at greater depths (Steinberg et al., 1970), while some species may completely lack cone photoreceptors (Hart et al., 2011, Schieber et al., 2012). Only a few benthopelagic and benthic species have been measured for temporal resolution, which shows a low threshold of 10–44 Hz (McComb et al., 2010, Kalinoski et al., 2014, Ryan et al., 2016, Ryan et al., 2017). Species with a higher temporal resolution tend to possess cone photoreceptors and occupy shallow coastal waters, while species with a lower temporal resolution, occupy dim light environments and possess rod dominated retinas (Hart et al., 2006).

There are no studies to date which have undertaken a comprehensive assessment of the visual adaptations of one species. In many cases this is because shark species that are readily available to capture from the wild are either too large or are otherwise too challenging to keep in captivity in large numbers and for extended periods. The blind shark *Brachaelurus waddi* (Figure 1) is a small

(adults typically 62-122 cm in total length, TL) benthic species found in abundance along the coast of Australia (DFL, 2009) and adapts well in captivity; this makes it amenable to recovery procedures that can allow an assessment of within-individual, trial-to-trial experimental variation over repeated experiments. Although *B. waddi* is commonly found in intertidal areas, such as rocky shore lines or seagrass beds, this species has been seen at depths up to 100 meters (Ebert et al., 2013). *Brachaelurus waddi* is a nocturnal species and preys on small fish, squid, and invertebrates, similar to Port Jackson shark, *Heterodontus portusjacksoni*, and the epaulette shark, *Hemiscyllium ocellatum* (Ebert et al., 2013). Little is known about its visual system, but it is expected to have vision that is well adapted to its nocturnal habit and its rather misleading common name 'blind shark' is due only to its tendency to retract its eyes when handled.

In this study, the anatomy and physiology of the visual system of *B. waddi* was investigated in order to better understand how the visual systems of sharks are shaped by specific ecological demands. Electroretinography was used to measure temporal resolution and contrast sensitivity over a range of light intensities. Temporal resolution was compared using two methods to establish the critical flicker fusion frequency (CFFF): a traditional sinusoidal stimulus of varying frequencies and a bandwidth-limited white noise stimulus. The spectral absorption characteristics of visual pigments in the retinal photoreceptors were measured using microspectrophotometry. Histological techniques were used to estimate spatial resolving power and identify any retinal specializations for high acute vision. Based on these results we were able to assess whether the visual system of *B. waddi* is correlated with behavioral adaptations and environmental constraints.

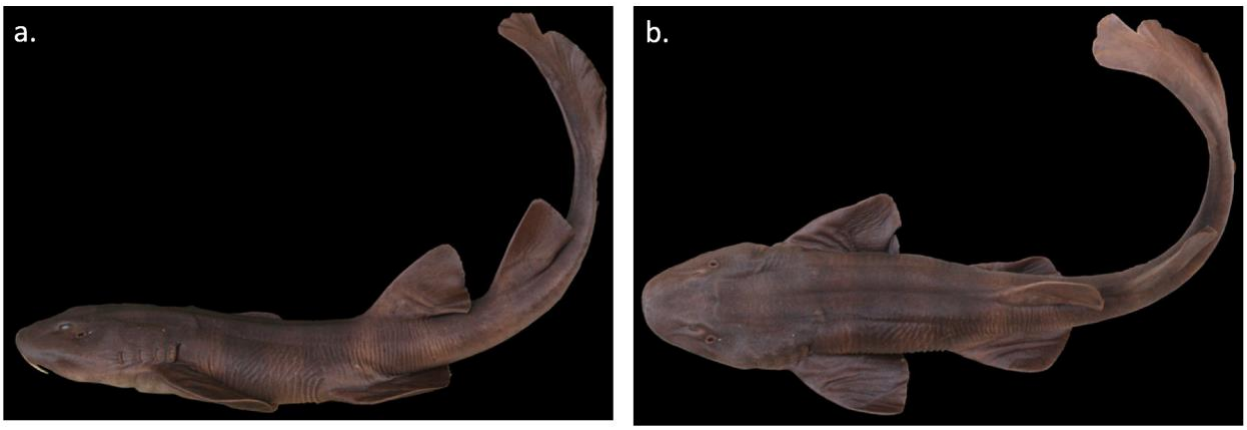

Figure 1: **a** Lateral photo of *Brachaelurus waddi* **b** Dorsal photo of *Brachaelurus waddi*. Total Length of shark is 45 cm. Images were retained with permission from Lawrence R. Frank, Digital Fish Library at UC San Diego: Scripps Institution of Oceanography Marine Vertebrate Collection Specimen number, SIO 91-87.

2. METHODS

2.1 Animals

Four adult (3 female, 1 male, total length, TL 23–60cm) and one juvenile (male, TL 13 cm) *B. waddi* were caught by line fishing in coastal waters off Sydney, New South Wales (NSW), Australia (NSW Department of Primary Industries and Fisheries scientific collection permit P17/0055-1.0) (Table 1). Male sharks were identified by the presence of claspers. Sharks were housed in recirculating seawater aquaria (400 L) for up to five months. All husbandry and experimental procedures were approved by the Macquarie University Animal Ethics Committee (Animal Research Authority 2017/039). Fresh tissue was necessary for MSP and topography, thus both eyes of an individual could not always be used for both techniques

Table 1: Individual *Brachaelurus waddi* total length, eye measurements and experiments summary. Transverse eye axial length and equatorial diameter were measured for individuals used in topography, whereas only axial length was measured in the other individuals.

Sex	Total length (cm)	Eye measurements (mm)			Experiments
		Left axial length - diameter	Right axial length - diameter	Lens	
male, adult	60.7	7.75	7.53	4.14	MSP
female, adult	26.2	7.97 (11.4)	8.40 (11.34)	5.06	ERG, Topography
female, adult	23.5	7.61 (13.76)	8.88 (13.68)	3.61	Topography
female, adult	55.5	7.64 (10.63)	7.64 (9.06)	4.05	ERG, MSP, Topography
male, juvenile	13.0	5.26 (6.81)	5.23 (6.81)	2.78	ERG, Topography

2.2. Electrophysiolgoy

Three *B. waddi* (Table 1) were used to estimate the temporal resolution and contrast sensitivity of the eye by measuring the electroretinogram (ERG) of the intact eye in response to a range of light stimuli. Electroretinography experiments were conducted in a dark room to prevent stray light from stimulating the retina. Once the shark had been dark adapted, all subsequent adjustments were made under dim red light using a head-torch fitted with a red light-emitting diode (LED). Sharks were dark-adapted for at least 30 minutes prior to being anesthetized to ensure the retina was in a state of dark adaptation and pupil was fully dilated. Once anesthetized, using 80–120 mg/L of ethyl 3–aminobenzoate methanesulfonate (MS222) buffered with an equal mass of sodium bicarbonate, the shark was transferred to a tank inside a Faraday cage and secured to an inclined stage using Velcro straps. The majority of the shark's body was submerged, and its eyes positioned out of the water. Oxygenated water containing a maintenance dose of 60–80 mg/L of MS222 buffered with an equal mass of sodium bicarbonate was pumped over the gills for the duration of the experiment via a plastic tube inserted in the mouth.

A recording electrode made of platinum wire (0.45 mm in diameter) with a small loop at the free end was dipped in conductive gel (Spectra 360 Electrode Gel, Parker Laboratories, INC.) and placed in contact with the surface of the cornea on the shark's left eye. A reference electrode made of chlorided silver wire (0.40 mm diameter) was inserted under the skin on the back of the head. An additional ground electrode was placed in the water surrounding the shark.

Light stimuli were generated using a high-power white LED, driven by a voltage-controlled current source. Light from the LED was delivered to the shark's eye via a 10 mm diameter liquid light guide (Oriel) that was terminated with an opaque diffuser (Lee Filter) located 30 mm from the left eye's corneal surface and aligned along the presumed optical axis of the eye. Fine control of light intensity was achieved by varying the voltage sent to the voltage-controlled current source, which provided a linear relationship between output light intensity and control voltage. Additional adjustment of light intensity was achieved using reflective quartz neutral density filters (Thorlabs, Inc.). Prior to presentation of the test stimulus, the eye was light adapted for 10 minutes at 50% of the maximum stimulus intensity used in the stimulus protocol at each light intensity/adaptation level, which was adjusted with a series of quartz $\log_{10}$ neutral density (ND) filters with nominal

ND values of 3.5, 2, 1, 0. The ND 3.5 filter provided the dimmest light intensity and ND 0 provided the brightest light intensity. Stimulus light intensities corresponding to these ND filter settings were measured as irradiance using a calibrated light meter, with irradiance at the brightest light (ND 0) measured as 3.34×10^{-4} W/cm^2 (International Light Technologies, ILT 1700).

Corneal voltages were amplified (×1,000) with an AC–coupled differential amplifier (DAM 50; World Precision Instruments, Inc, City), with high pass and low pass cut-off frequencies at 0.1 Hz and 1,000 Hz, respectively. A 'Hum Bug' (Quest Scientific Instruments Inc.) was inserted in the signal pathway after the amplifier to reduced 50 Hz mains noise. Amplified and filtered voltages were digitized using a National Instrument (USB–6353 X-series) data acquisition device, the same device as used to control the stimulus light to elicit the electroretinogram. Data acquisition and light stimuli were controlled using custom software written (Nathan Hart) in Microsoft Visual Basic using DAQmx libraries provided by National Instruments.

2.2.1. Temporal Contrast Sensitivity

Temporal resolution was tested by measuring the critical flicker fusion frequency (CFFF) at four different light intensities (ND, 3.5, 2, 1 and 0). The CFFF threshold was determined by recording the response of the retina to increments of increasing temporal frequencies. The CFFF was considered to have been reached when the stimulus frequency was increased to a point where the retina was no longer able to respond in a synchronous fashion. The light stimuli were presented as a sinusoidally modulated stimulus (SMS) of 5 seconds duration and 95% Michelson contrast. Frequencies below 7 Hz were tested in increments of 2 Hz (3 Hz, 5 Hz, 7 Hz), followed by increments of 5 Hz at frequencies between 10 Hz and 40 Hz. Every other frequency was tested in increasing order (10Hz, 20 Hz, 30 Hz, 40 Hz) until no response at the test frequency was recorded, and then the skipped frequencies were tested in decreasing order (35 Hz, 25 Hz, 15 Hz) to monitor any changes in the preparation over time. Control measurements were made at each light intensity by blocking the light stimulus and recording the response at each temporal frequency tested from 5 Hz to 40 Hz at 95% contrast. These measurements were used to determine the baseline noise threshold for both temporal and contrast sensitivity.

Contrast sensitivity was tested at each temporal frequency by presenting a series of stimuli of decreasing contrast, starting at 95% contrast and approximately halving each step (i.e. 95%, 50%, 25%, 12.5%, 6.25%) until no response was recorded. Each light stimulus for both temporal frequency and contrast sensitivity was presented 15 times and averaged to obtain a mean response. This was displayed during the experiment in both the time domain and the frequency domain (by way of a Fast Fourier transform) such that the amplitude at the test frequency could be evaluated.

Analysis of ERG amplitudes for SMS followed established methods (Ryan et al., 2017). To ensure the CFFF and contrast threshold had been reached, two additional stimuli beyond the apparent thresholds were presented. A custom (Laura Ryan) MATLAB script (Natick, MA, USA) adapted from Ryan et al. (2017) was used to assess whether the amplitude of the FFT response differed significantly from that of five frequency amplitudes on either side of the frequency peak. The noise threshold was defined as the average of the controls plus two times standard deviation. Contrast threshold was established at each temporal frequency by interpolating between the last response above the noise threshold—the FFT amplitude of which was also significantly greater than the five frequencies on either side—and the first point below the noise threshold. (Fig. 2a). A temporal contrast sensitivity curve was plotted for each light (Fig. 2b, c), where contrast sensitivity is the reciprocal of contrast threshold, such that a contrast sensitivity of 10 is equivalent to a contrast threshold of 0.1 or 10%

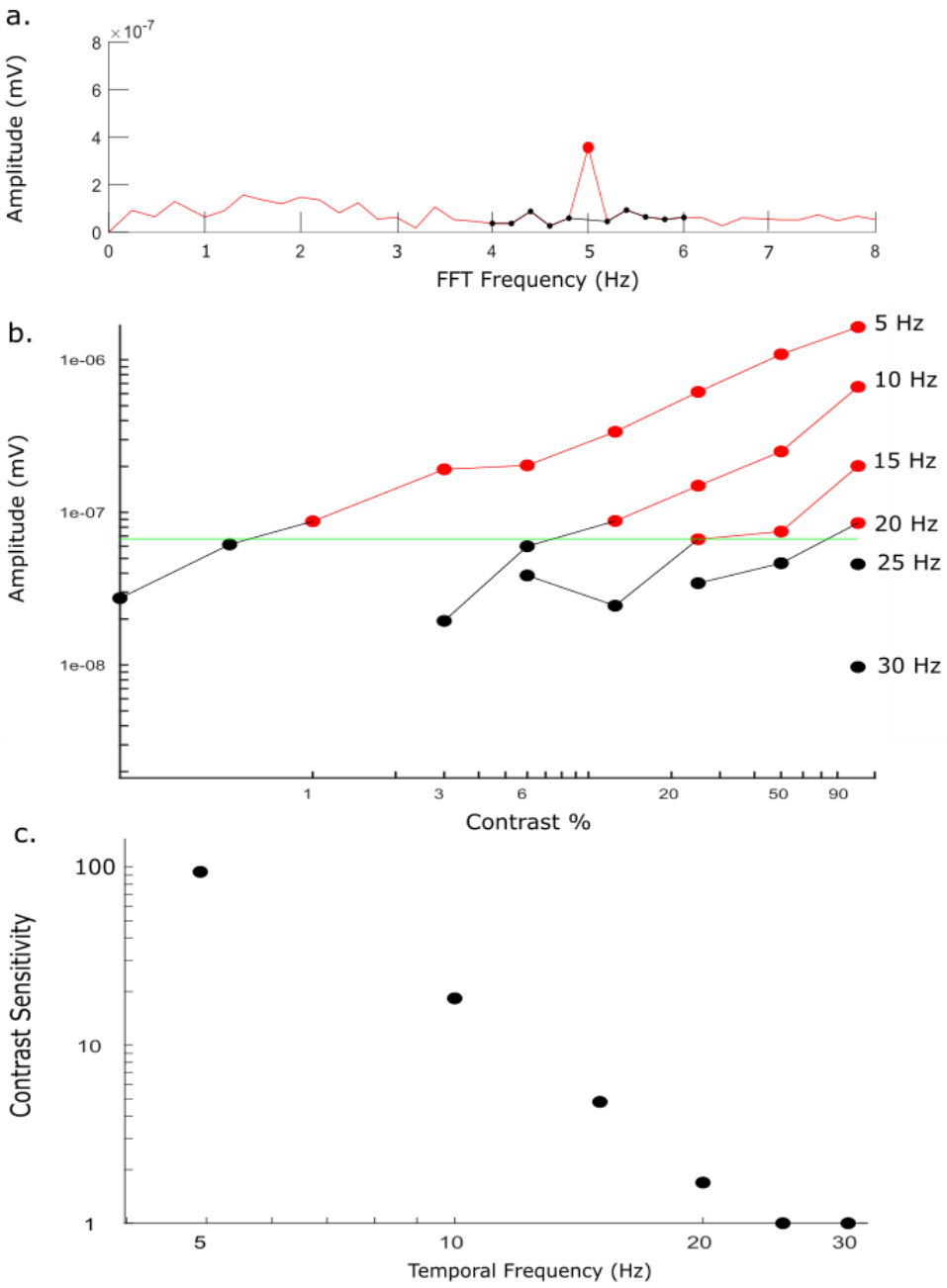

Figure 2: Example of critical flicker fusion frequency recordings from sinusoidal modulated stimulus presented at an ND 0 from one individual of *B. waddi.* **a.** FFT analysis that measured the response amplitude to a SMS stimulus presented at 5 Hz (red circle) at 95% contrast. The five frequencies on either side (black circles) were used to determine whether the amplitude at 5 Hz was a significant response compared to the background noise. **b.** Response amplitudes to different contrast (red circles) presented at six temporal frequencies (red line: top-bottom, 5 Hz, 10 Hz, 15 Hz, 20 Hz, 25 Hz, 30 Hz). Green line represents noise threshold. Black circles represent amplitudes to contrast that were not significantly different from the background noise or ten surrounding frequencies. **c.** Temporal contrast sensitivity curve- inverse of contrast threshold- from the same individual at ND 0.

The effects of light intensity and temporal frequency on contrast sensitivity and the CFFF thresholds were analyzed in R (Version 1.1.456–© 2009–2018 RStudio, Inc.) using a mixed model analysis and package 'lme4' (Bates et al., 2013). The significance of the models was compared using analysis of variance (ANOVA). Shark identity was treated as a random factor in the models. When assessing the effect of light intensity on temporal contrast sensitivity, light intensity and temporal frequency were treated as categorical variables due to the non-linear relationship between contrast sensitivity and light intensity. This also allowed for a comparison to be performed to determine the relationship between light intensity, temporal frequency and contrast sensitivity. To apply the assumption of homogeneity of variance (Zar, 1999), temporal resolution and contrast sensitivity was calculated to $\log_{10}$–transformed for the analysis.

2.2.2. Critical Flicker Fusion Frequency: White Noise Stimulus

Estimates of temporal resolution for *B. waddi* generated using the SMS were compared to those obtained using an alternate, and potentially more rapid method, i.e. a bandwidth-limited binary white noise stimulus (hereafter referred to as WNS). This approach has been used previously to characterize the physiology of neural systems, including the retina (Marmarelis and Marmarelis, 1978). Since the WNS was a new technique for use in sharks, the methodology was first developed using additional experimental models to assess hardware and technique: one male epaulette shark, *Hemiscyllium ocellatum* and five Australian bull ants, *Myrmecia midas*. This development work formed part of the present thesis and although not discussed in detail here is described in Appendix A.

The WNS was generated using a custom MATLAB code (Nathan Hart) and consisted of a pseudorandom (on/off) binary sequence (on = 100% light intensity, off= 0% light intensity) that controlled the operation of the stimulus LED. The update rate of the LED driver voltage was such that the frequency bandwidth of the WNS was 0–64 Hz. The same WNS was used in every recording so that repeated recordings could be averaged in the time domain to improve the signal to noise ratio.

Immediately following each ERG recording using the SMS, the eye was light adapted at 50% light intensity (i.e. the time-averaged mean of the on and off light intensities) for 10 minutes prior to

presentation of the WNS. The WNS lasted 48 seconds. Recordings continued after the WNS stopped, for an additional 47 seconds with the LED providing the same adapting light (50% light intensity) as that prior to the WNS stimulus. The total recording time thus lasted 95 seconds and the WNS was repeated 10 times at each light intensity. Response were amplified, filtered and digitized with the same parameters used for the SMS recordings (see above).

Individual recordings at each light intensity were inspected for artefacts (i.e. spurious full-scale peaks or troughs due to movement of the animal or excessive electrical noise) in MATLAB (R2018a) and acceptable records averaged for each light intensity. The averaged response data (and WNS) were then trimmed to remove the first 5 seconds after onset of the WNS to exclude any ON-response and the last 3 seconds to give a recording epoch of 40 seconds for further analysis.

To determine the highest frequency at which the retina was no longer able to respond to the WNS, the stimulus and matching response data were analyzed using the *mscohere* function in MATLAB. The *mscohere* function estimates the magnitude-squared coherence between two ERG responses using Welch's averaged, modified periodogram method (Welch, 1967, Rabiner and Gold, 1975). Both the WNS approach and magnitude squared coherence analysis assume that the system under consideration is both linear and time-invariant. Neither the response properties of the whole retina nor the individual neurons that contribute to the ERG and the visual process are linear across their entire operational range and the assumption of time-invariance may be violated depending on dynamic changes in adaptation state. However, this approach may still provide a useful approximation for the visual system when the linear component of the response dominates over the non-linear components, as is typically the case with retinal neurons and the ERG (Marmarelis and Marmarelis, 1978, Hemmi et al., 2002, Zele et al., 2017). A similar approach has been used to estimate the frequency response bandwidth of other sensory systems (Infantosi et al., 2006).

The magnitude-squared coherence estimate at all frequencies was low past filtered using a zero phase-shift Butterworth filter with a corner frequency of 512 Hz to smooth noise in the data. A noise threshold was estimated by calculating the upper 95% confidence interval for the parameter estimates on the mean and standard deviation for the magnitude squares coherence estimate at a

range of frequencies well beyond the likely CFFF of the retina (i.e. 128 to 256 Hz) using the MATLAB *normfit* function. The point at which the smoothed magnitude-squared coherence function crossed this value was taken as the highest frequency within the WNS to which the retina could respond, i.e. the alternate CFFF estimate.

The CFFF estimates made using the SMS and WNS methods were compared in R (version Rx64 3.4.0) using a mixed model analysis and package 'lmer' (Bates et al., 2013). Shark identity was treated as a random factor and the significance of the models was compared using ANOVA.

2.2. Microspectrophotometry

One eye from each of two *B. waddi* (Table 1) were used to measure the spectral absorption properties of retinal photoreceptors using microspectrophotometry (MSP). Sharks were dark adapted for one hour prior to being euthanized with an overdose of MS222 (500mg L^{-1} buffered with an equal mass of sodium bicarbonate). Immediately following euthanasia, retinae were removed and placed in an elasmobranch physiological saline solution (330 mmol 1^{-1} urea, 350 mmol 1^{-1} NaCl, 4 mmol 1^{-1} KCl, 5 mmol 1^{-1} $CaCl_2$, 2 mmol 1^{-1} $MgCl_2$). All dissections were done under infrared illumination as described elsewhere (Hart et al., 2004). Briefly, retinae removed from excised eyes were cut into small pieces (~1mm^2) and mounted onto a glass coverslip (Menzel-Gläser No. 1, 24 × 60 mm) in a drop of elasmobranch solution containing 10% dextran. The preparations were covered with a coverslip (Menzel-Gläser No. 0, 22 × 22 mm) and the edges of the coverslip were sealed using clear nail polish to prevent dehydration (Shand et al., 2002).

Transverse absorption spectra of photoreceptor outer segments were measured using a single-beam wavelength-scanning microspectrophotometer (Hart, 2004, Hart et al., 2011). A sample scan was first made by adjusting the dimensions of the measuring beam to fit inside the outer segment and scanning through the spectrum (330 nm–800 nm). The dimensions of the beam varied depending on the size of the outer segment, but were typically 21×2 μm. A baseline scan was recorded subsequently in a cell-free area adjacent to the photoreceptor. A pre-bleach spectrum was created by subtracting the baseline scan from the corresponding sample scan and converted to absorbance. Photoreceptors were then bleached for two minutes with full spectrum 'white light' from the monochromator, and subsequent sample and baseline scans made to create a post-bleach spectrum

and confirm the pigment measured in the outer segment was photolabile. Difference spectra were created for each outer segment by subtracting the post-bleach spectrum from the pre-bleach spectrum. Scans were analyzed as described elsewhere (Hart et al., 1998, Govardovskii et al., 2000, Hart, 2002) and scans meeting established selection criteria were retained for further analysis (Levine and MacNichol, 1985).

2.3. Topography and Spatial Resolving Power

The topographic distribution of ganglion cells was assessed in four individual *B. waddi* (Table 1). In each case, the retinas from the left eye were obtained from individuals that had been euthanized with an overdose of MS222 (500 mg L^{-1} buffered with an equal mass of sodium bicarbonate). Retinal wholemounts were made following established techniques (Ullmann et al., 2012) with minor modifications outlined below.

Immediately following euthanasia, a mark was made on the dorsal side of the sclera to orientate the eye once removed from the head. The axial and transverse length of the eye was recorded (Table 1) using an electronic digital caliper. Once the cornea was removed, the diameter of the lens was recorded (Table 1) and the eyecup was fixed in 4% paraformaldehyde (0.1M phosphate buffer pH 7.4) and stored in a refrigerator (≈ 4°C) for a minimum of twenty-four hours.

Following fixation, the retina was teased away from the eye cup in phosphate-buffered saline (0.1M PBS pH 7.3) and flat mounted, ganglion cell layer uppermost, onto gelatin-coated glass slides (76×51×1 mm, clear white glass ProSciTech). Retinas were then placed in an air-tight chamber and fixed to the slide by exposure to 16% paraformaldehyde vapors at ≈ 60°C for one hour. Once cooled and allowed to dry overnight, the whole-mounts were rehydrated through a descending alcohol series, followed by distilled water, then stained with 0.05% Cresyl Violet acetate (pH ~4) for 10–25 minutes. After staining, whole-mounts were rinsed in distilled water and dehydrated through an ascending alcohol series. Following Lisney and Collin (Lisney and Collin, 2008), whole-mounts were cleared in xylene for 30 minutes then mounted in Entellan®New and sealed with a clear glass coverslip (50×32 mm, No. 1; ProSciTech).

The stained whole-mounts were examined following established methods (Cohn et al., 2015), using a Olympus BX63 microscope and automatic stage with a digital camera coupled with a cellSens Imaging Software (Olympus 1.12). An enlarged overlay of the retina was created using 20× magnification objective lens. The overlay was calibrated with landmark coordinates (upper-, lower-, right-, and left-most margins of the retina) at 100× magnification objective lens and fitted with a coordinate grid, which served as a reference for counting positions (Ullmann et al., 2012). Counting positions were made within a defined counting frame (100×100 μm) at 100× magnification objective lens. All the cells inside the counting frame were counted, except for any cell that touched the left most or lower most walls of the frame (Gundersen, 1977, Coimbra et al., 2009, Garza-Gisholt et al., 2015). Following Collin and Pettigrew (1988) all stained cells in the ganglion cell layer were counted, except for recognizable glial cells, largely because in areas of high cell density it was difficult to distinguish between displaced amacrine cells and small ganglion cells. Thus, the counts obtained represent the upper-most estimate of ganglion cell density. The counting frame positions were established at 500 μm intervals across each retina. Depending on the size of the retina, a total of 337-390 frames were counted per retina in adult *B. waddi* and 136 frames counted in the retina of the juvenile *B. waddi.*

To map the topographic distribution of ganglion cells in the retina, the number of cells per counting position were converted to cell density per square millimeter. An outline of the retina (from the enlarged overlay image) was created, saved as an ImageJ Region of Interest (ROI.file) and an outline of the optic nerve was traced and saved as x-, y- coordinate file using ImageJ (version 1.52a, National Institutes of Health, USA). Landmark and counting positions were converted to corresponding pixel coordinates from the outline on ImageJ. The orientation and cuts on the outline of the retina were marked and the retina was reconstructed in RStudio (Version 1.1.456-© 2009-2018 RStudio, Inc.) using the package 'retistruct' (Sterratt et al., 2013) to recreate the original form of the curved retina as it would sit in the eye cup. A topographic map of the retina was created by projecting count data onto the outline of the retina in the RStudio package 'retina' and plotted with iso-density contours (Cohn et al., 2015).

Based on the peak density of neurons counted in the GCL, the anatomical spatial resolving power of the eye was calculated using equations 1–4 and assuming a hexagonal packing arrangement of neurons in the retinal mosaic (Matthiessen, 1880, Hart, 2002, Theiss et al., 2007)

(1) $d = \frac{2\pi f}{360}$

(2) $S^2 = \frac{2}{D\sqrt{3}}$

(3) $v = \frac{1}{S\sqrt{3}}$

(4) $v \times d = SRP$

Where d is the distance subtended by one degree on the retina, f is the focal length calculated by multiplying the axial radius of the lens by Matthiessen's ratio. A ratio of 2.75 was used given it is specific for sharks, rather than the value of 2.55 that is obtained from teleost fishes and whose eye structure differs optically. S is the cell to cell spacing in the retina, D is the maximum ganglion cell density in the retina, v is the maximum spatial frequency, and *SPR* (Spatial Resolving Power) in cycles per degree (*cpd*).

3. RESULTS

3.1. Electrophysiology

3.1.1. Temporal Contrast Sensitivity

The contrast sensitivity in *B. waddi* was greatest at lower temporal frequencies and decreased at higher temporal frequencies (Figure 3). Contrast sensitivity increased with light intensity, but not at a linear rate (mixed model, temp × intensity, Chi-sq$_1$= 97.706, degrees of freedom=8, *P* value= <0.001). At the dimmest light intensity, the contrast sensitivity curve was lowest and at the brightest intensities the contrast sensitivity curves were similar (Figure 3). For example, at 5 Hz the contrast sensitivity measured at ND 0 (177.6 ±43.4, equating to a contrast threshold of 0.56%) did not differ significantly from the contrast sensitivity measured at ND 1 (205.2 ±134.3,

0.49%) (Tables 2, 3). The contrast sensitivity threshold (mean highest contrast sensitivity for each individual at any stimulus intensity and frequency) for *B. waddi* was 222.2 ±120.0, 0.45%.

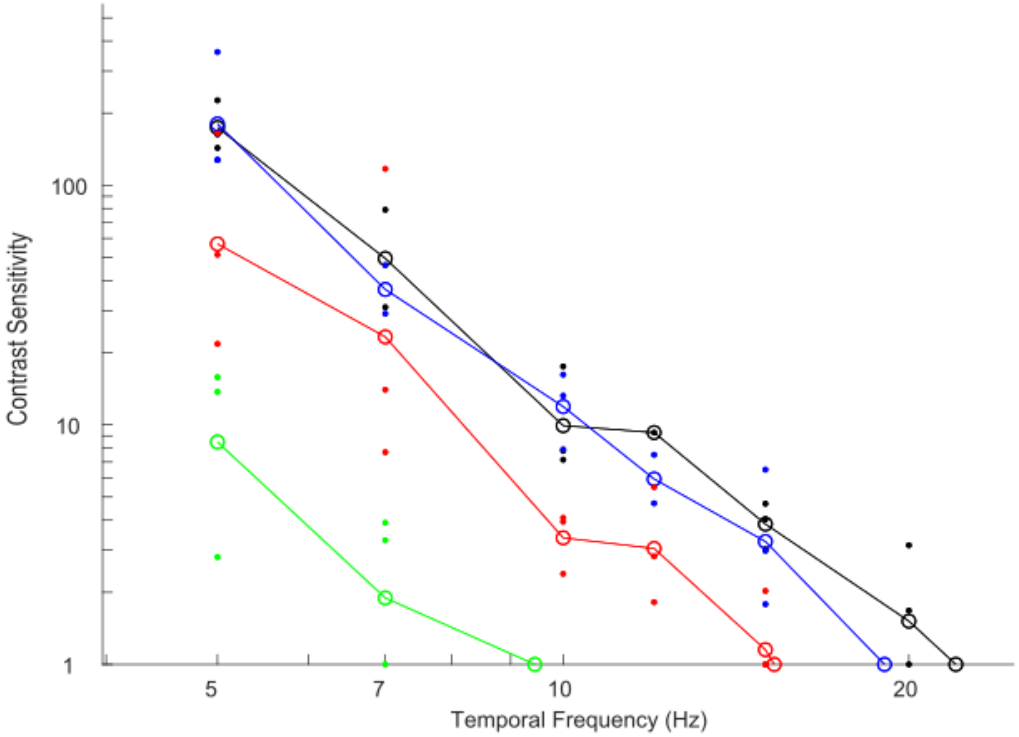

Figure 3: Mean (open circles) and individual estimates (closed circles) of temporal contrast sensitivity in *B. waddi* (n=3) at four light intensities (ND filters: 0=black, 1=blue, 2=red, 3.5=green)

Table 2: Results of the multiple comparisons between contrast sensitivity estimates at different light intestines at three temporal frequencies (5 Hz, 7 Hz, 10 Hz). The light intensity represents the ND filter comparison (ND 0, 1, 2, 3.5). The degrees of freedom (df), t-ratio, and *P* values are presented. * Statistically significant results at *P* <0.05

Light	5 Hz		7 Hz		10 Hz	
Intensity	t-ratio	*P* value	t-ratio	*P* value	t-ratio	*P* value
0=1	-0.084	0.99	0.59	0.93	-0.45	0.97
0=2	2.73	0.04*	1.61	0.38	2.64	0.05
0=3.5	7.39	<0.01*	6.62	<0.01*	4.81	0.01*
1=2	2.82	0.03*	0.96	0.77	3.08	0.02*
1=3.5	7.48	<0.01*	5.96	<0.01*	5.25	<0.01*
2=3.5	4.66	0.01*	5.62	<0.01*	2.17	0.15

Temporal threshold increased with increasing light intensity (Figure 3) (mixed model, Chi-sq$_1$= 7.70, degrees of freedom=1, *P* value= 0.005). The maximum temporal threshold estimated using the SMS was approximately 22 Hz (± 2.13) for *B. waddi* (n=3; Table 3).

3.1.2 Critical Flicker Fusion Frequency

When comparing the CFFF estimates obtained with the WNS and SMS methods, both increased with light intensity (mixed model, Chi-sq$_1$= 20.6, *P* value= <0.001). The temporal threshold for SMS (22 Hz ± 2.13 SD and WNS (17 Hz ± 2.28 ± SD) were not significantly different at any light intensity tested (mixed model, method + intensity, Chi-sq$_1$= 1.83, *P* value= 0.1761). (See Appendix A. for comparison of WNS and SMS in two other model species *Hemiscyllium ocellatum* and *Myrmecia midas*).

Table 3: The mean (± 1 standard deviation), critical flicker fusion frequency (CFFF) for sinusodal modulated stimulus (SMS, Hz), temporal threshold using the white noise stimulus (WNS, Hz) and contrast sensitvity (CS) threshold (at 5 Hz) at the four relative light intensities for *Brachaelurus waddi* (n=3).

	CFFF		CS (5 Hz)
Light Intensity (ND)	SMS	WNS	
0 (brightest)	22 (± 2.13)	17 (± 2.28)	177.6 (±43.4)
1	19 (± 0.87)	15 (± 2.64)	205.2 (± 134.3)
2	15 (± 1.67)	14 (± 2.00)	79.3 (± 75.5)
3.5 (dimmest)	9 (± 2.42)	12 (± 3.21)	10.8 (±6.9)

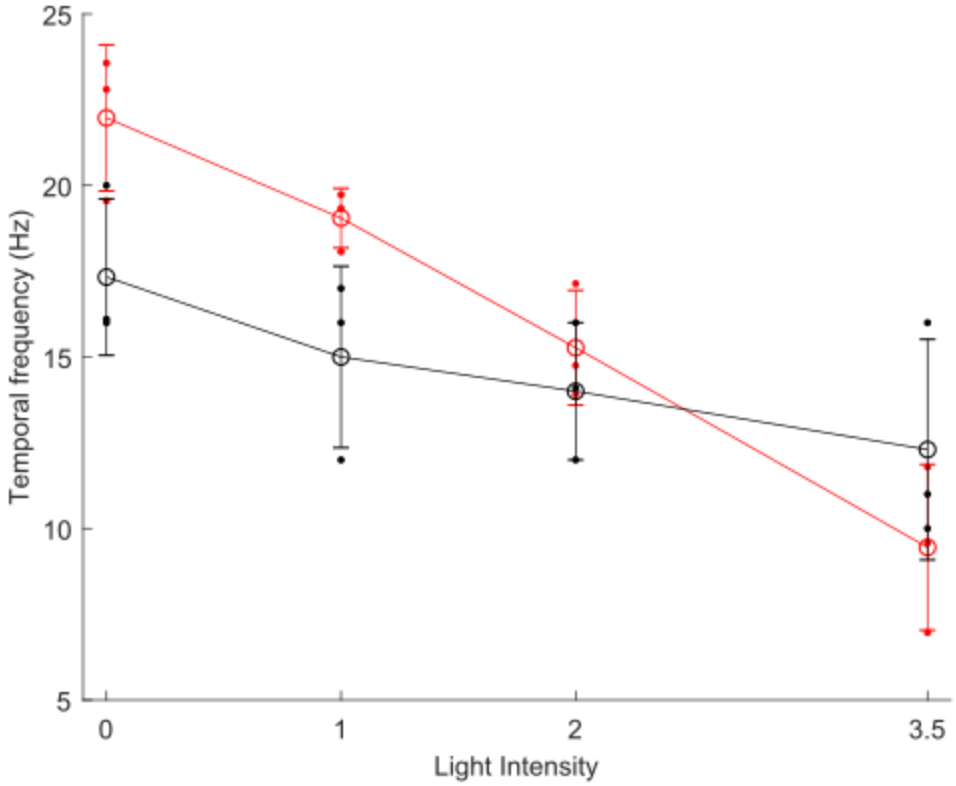

Figure 4: Estimated critical flicker fusion frequencies (CFFF) at 4 different light intensities for *B. waddi* using a white noise stimulus (WNS; black dots represent individual means, black open circles represent species mean and bars show +/- 1 standard deviation) and sinusoidal modulated stimulus (SMS; red, dots represent individual means, black open circles represent species mean and bars show +/- 1 standard deviation).

3.2. Microspectrophotometry

The *in situ* spectral absorbance properties of the visual pigments located in the retinal photoreceptors of *B. waddi* were measured from two individuals (Table 1). Rods were the only type of photoreceptor identified in the retina (Table 4). Absorbance spectra were recorded from 106 rods; of these, 42 cells were retained and used to calculate the mean absorbance spectra. The rods contained a medium-wavelength ('green') sensitive visual pigment (Figure 5) with a mean λ_{max} at 501 nm (Table 4). All absorbance spectra were fitted best by a vitamin A1-based (rhodopsin) visual pigment template (Govardovskii et al., 2000).

Table 4: Spectral absorbance properties in the rod photoreceptors of *Brachaelurus waddi*, measured using microspectrophotometry. Values are ± 1 standard deviation. λ_{max}, wavelength of maximum absorbance.

Rod photoreceptors	
Mean pre-bleach λ_{max} (nm)	500.9 ± 2.0
λ_{max} of mean pre-bleach spectrum (nm)	500.6
Mean difference spectrum λ_{max}	504.0 ± 3.3
λ_{max} of mean difference spectrum (nm)	504.1
Mean transverse absorbance change at λ_{max} of difference spectrum	0.017 ± 0.004
Number of cells averaged for pre-bleach spectrum	42
Number of cells averaged for difference spectrum	46
Outer segment length (μm)	21 ± 3.0
Outer segment diameter (μm)	2 ± 0.3

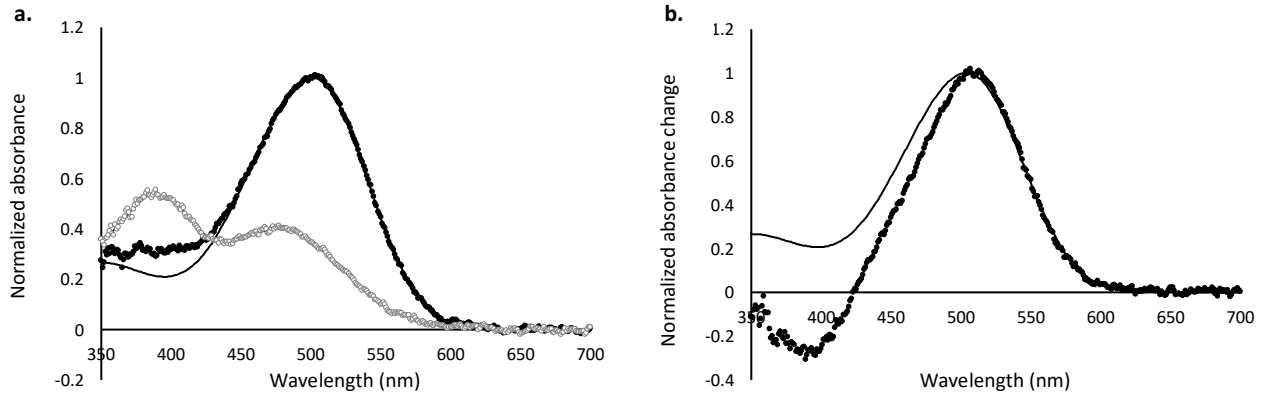

Figure 5: **a** Normalized mean pre-bleach (black symbols) and post-bleach (grey symbols) absorbance spectra of the rod (n=42 cells) visual pigment in *B. waddi* with rhodopsin visual pigment template of the appropriate λ_{max} (solid line) and running average (dotted line), respectively. **b** Normalized mean difference spectrum (black symbols) with corresponding rhodopsin visual pigment template (solid line).

3.3. Topography and Spatial Resolution

3.3.1. Topography

Topographic maps of the reconstructed retinas of the four *B. waddi* examined (Table 1) showing changes in density of neurons in the ganglion cell layer across the retina are displayed in Figure 6. Cell densities varied from <200 cells per mm^2 at the retinal periphery to >1400 cells per mm^2 in the regions of highest density. Inspection of the maps revealed a weakly defined, elongated horizontal band or streak of higher cell density in the central-dorsal region of the retina (Figure 6). The shallow gradient in cell density likely means that small variations or errors in cell counts have a big effect on the shape of the contours that are formed by the package, which in turn affect the apparent shape of the specializations on the retina. It is likely that the retina shrank slightly throughout the fixation and staining process, but as this typically occurs mostly at the periphery of the retina or cut edges, the count data were not corrected for shrinkage.

According to the documentation of the 'retina' code in R used to create the maps (Cohn et al., 2015) it is possible to make composite maps but we were unable to use this functionality to create an average of the four retinas; however, this might be possible in future and may help to further clarify the distribution of retinal neurons. An average map will be created for future publication.

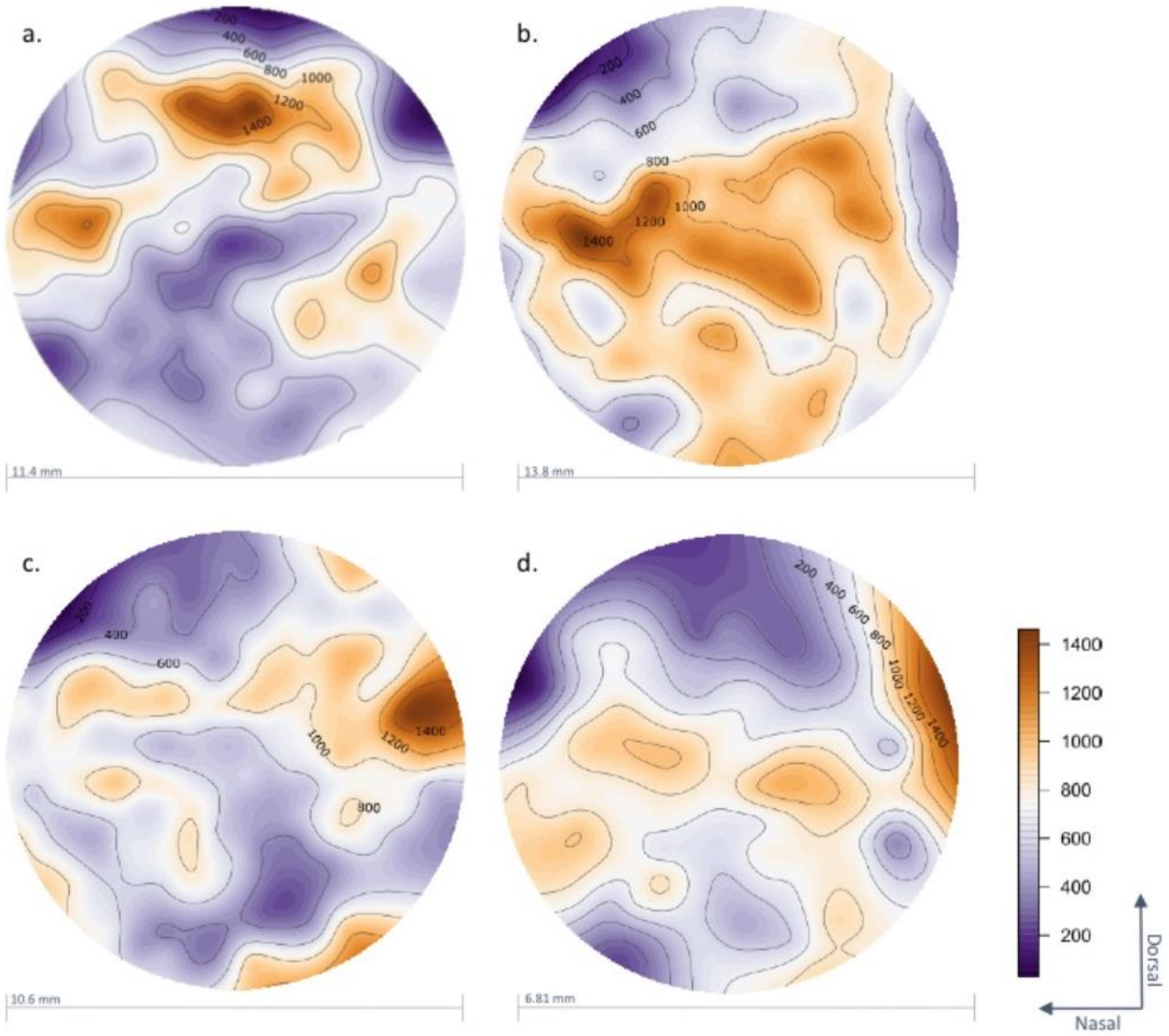

Figure 6: Topographic distribution of Nissl-stained neurons in the ganglion cell layer of the left retina in four *B. waddi* (orientation: dorsal top, nasal left). Retinae were reconstructed from flattened whole-mounts assuming a spherical shape and the equatorial diameter of each eye is indicated. Isodensity contour lines are shown and labels represent boundary densities in cells per mm^2. A color heat map is shown to assist in visualization of changes in cell density across the retina.

3.3.2. Spatial resolving power

A mean value was calculated for peak ganglion cell density, focal length, and spatial resolving power. Focal length was based on lens radius and a Mattheissens ratio (2.75) for elasmobranchs

(Litherland and Collin, 2008, Theiss et al., 2012). The peak ganglion cell density in the elongated horizontal streak of the dorsal region of the retina reached an average of approximately 2175 cells/mm^2 (±512 SD) (Figure 6). The focal length of the eye was similar between the four individuals with a mean of 5.21 mm (±1 SD). The peak density was used to estimate the mean spatial resolving power, which was 2.36 cycles per degree (cpd) (±0.4 SD; n = 4)

4. DISCUSSION

4.1. General remarks

Several important characteristics of the visual system of *Brachaelurus waddi* were measured, namely temporal resolution and contrast sensitivity, the spectral absorbance properties of the rod visual pigment, the anatomical spatial resolving power and topographic distribution of neurons in the ganglion cell layer. The results confirm that *B. waddi*, otherwise known as the 'blind shark', is in fact not blind (!) and possess several visual adaptations that reflect its behaviour and habitat.

4.2. Temporal resolution

The temporal resolution and contrast sensitivity of three *B. waddi* were measured using electrophysiological techniques. Temporal resolution in *B. waddi* ranged from 9 Hz at the dimmest light intensity to 22 Hz at the brightest when measured using the SMS method (for a comparison with the WNS method, see below). Slight differences in temporal resolution might be due to differences in stimulus light intensity between experimental set-ups, adaptation levels of the eye, prolonged anesthesia, or water temperature (Frank, 2000, Fritsches et al., 2005, Bedore et al., 2013). However, the results for this species are considered to be robust given that the CFFF threshold obtained for *H. ocellatum* (40 Hz; see Appendix A) is similar to that obtained in a previous study using slightly different equipment (Ryan et al 2017).

Temporal resolution measured from the whole retina using electroretinography likely reflects the photoreceptor composition of the retina. Rod photoreceptors have longer integration times compared to cone photoreceptors; longer integration times (i.e. lower temporal resolution/CFFF) decrease the eye's ability to resolve rapidly changing images such as those generated by a moving object which, as a result, may influence behaviors such as prey capture (Dowling and Ripps, 1970). Similar to *H. portusjacksoni* (CFFF 28 Hz) (Ryan et al., 2017), *B. waddi* has a rod dominated

retina (see below) and generally feeds on sessile prey such as small crustaceans (Schieber et al., 2012). In contrast, species with lower rod-to-cone ratios, such as *H. ocellatum* (18:1) (Schieber et al., 2012) have higher temporal resolution (40 Hz) and often feed on more active prey (i.e. fish) (Foged and Powter, 2015). Thus, the finding of a low temporal resolution in *B. waddi*, potentially supports the association between temporal resolution and prey type (McComb et al., 2009, Schieber et al., 2012, Ryan et al., 2017).

Furthermore, species with lower temporal resolution tend to occupy dimly lit environments (Dowling and Ripps, 1970). *Brachaelurus waddi* can be found in dimly lit caves and at depths up to 100 meters (Ebert et al., 2013). Similarly, a correlation between low temporal resolution and dimly lit environments is seen in *H. portusjacksoni*. *Heterodontus portusjacksoni* is a nocturnal species with a typical habitat depth range >100 meters and has a low temporal resolution (Ryan et al., 2017). In contrast, shallow dwelling species (<100m), such as *H. ocellatum*, have a higher temporal resolutions or tend to inhabit coastal reefs, thus experiencing greater light intensities (Gramoni and Ali, 1970).

Temporal resolution provides insight to an animal's ecological demands, such as prey selection and habitat. A high temporal resolution suggests an animal may occupy bright light environments, such as coastal reefs, or predate on fast moving prey. As opposed to a low temporal resolution which suggest an animal inhabits a dimly lit environment or hunts slow moving prey. However, the small number of species investigated to date (McComb et al., 2010, Kalinoski et al., 2014, Ryan et al., 2015, Ryan et al., 2016) makes it hard to predict temporal resolution solely on behavioral adaptations or environmental influences. In order to better associate such aspects of retinal physiology with life history, a wider range of species, such as pelagic sharks, should be studied. A better understanding in a range of sharks could provide insights into the visual abilities of sharks associated with attacks on humans, such as the great white shark *Carcharodon carcharias*, the bull shark *Carcharhinus leucas*, and the tiger shark *Galeocerdo cuvier*. However, there are many difficulties in catching and studying such species in a laboratory setting and future research might focus on different methodological approaches to measure temporal resolution in such species, for instance performing ERG on fresh excised eye cups from specimens collected opportunistically. The abbreviated WNS stimulus protocol may be useful in this regard.

4.3. Contrast sensitivity

High contrast sensitivity in *B. waddi* (0.56%) likely reflects the need for good vision in a low contrast marine environment. *Brachaelurus waddi* can be found in seagrass beds, and rocky, sandy floors in the intertidal areas (Ebert et al., 2013). These types of aquatic habitat are affected by substantial daily fluctuations in the turbidity of the water (Warrant and Johnsen, 2013). Water turbidity is the measure of cloudiness in the water due to suspended particles. (McFarland and Loew, 1883). In intertidal areas, where a lot of plants, sand, shells, and mud are continually breaking up and moving around in the water column, water visibility can be limited to less than a meter, and high contrast sensitivity would be critical for visually mediated prey detection and predator avoidance under such conditions. In contrast, species such as the brownbanded bamboo shark, *Chiloscyllium punctatum* (contrast sensitivity 2.4%) (Ryan et al., 2017) that occupy areas less affected by water turbidity (i.e. coral reefs and intertidal pools) (Harahush et al., 2009) have lower contrast sensitivity.

4.4. Microspectrophotometry

In this study, only rod photoceptors were found in the retina of *B. waddi*. It is possible that cone photoreceptors were present but missed during sampling. All-rod or rod-dominated retinas are thought to be a strategy to improve vision in dim light environments. All-rod retinas are found in some strongly nocturnal skates (Dowling and Ripps, 1970, Pepperberg et al., 1978) and sharks, such as *H. portusjacksoni* (Schieber et al., 2012) and those that live at considerable depths, e.g. XXXX (ref), whereas shallow water benthic shark species possess cones photoreceptors, though at relative high rod:cone ratios, for example the *H. ocellatum* (18:1 peak) (Schieber et al., 2012) and the ornate wobbegong *Orectolobus ornatus* (19:1 peak) (Litherland and Collin, 2008). Although this study did not allocate time or tissue to be certain *B. waddi* has an all-rod retina it would be beneficial for understanding visual adaptations relative to the ecological demands. This can only be properly resolved with further anatomical or molecular genetic studies to identify cone photoreceptors.

The λ_{max} of rod photoreceptors, and in some cases cone visual pigments, is generally related to the spectral distribution of light in the habitat. As depth increases and the spectrum of light becomes

narrower, fish tend to show shifts in λ_{max} that match the dominant wavelengths. Moreover, the direction of the shift is dependent on water type; whereas pelagic species tend to show shifts toward (bluer) wavelengths (λ_{max} approximately 470-490 nm) and estuarine and freshwater species tend to be tuned to longer (redder) wavelengths (λ_{max} 497-510 nm) (Hart et al., 2006). Although *B. waddi* has been seen at depths greater than 100 meters, relatively little is known about where it spends the majority of its time. The wavelength of maximum absorbance (λ_{max}) of the visual pigment located in the rod photoreceptors of *B. waddi* (500 nm) is similar to other shallow water marine species such as *H. ocellatum* (λ_{max} 499 nm) and *O. ornatus* (λ_{max} 498 nm). Thus, suggesting *B. waddi* to be a predominately shallow water inhabitant.

4.5. Topography and Spatial Resolution

The topographic distribution of ganglion cells in *B. waddi* showed a weakly defined, elongated horizontal band or visual streak of higher density in the central-dorsal region of the retina. The significance of the visual streak allows an animal to scan a broad area with increased spatial resolving power (i.e. ability to discriminate between small objects or fine detail) and minimal eye movement (Hughes, 1971, Bozzano and Collin, 2000, Lisney et al., 2012, Schieber et al., 2012). The location and size of the streak differs among species (Bozzano and Collin, 2000, Bozzano, 2004, Litherland and Collin, 2008, Schieber et al., 2012). A dorsal horizontal streak is generally seen in benthic species (Collin and Pettigrew, 1988, Bozzano and Collin, 2000, Bozzano, 2004), such as *H. ocellatum* (Last and Stevens, 1994) and *H. plagiosum* (Yew et al., 1984) . Benthic species rest on the substrate and look sideways and upwards. Thus, a streak located in the dorsal region of the eye would improve the animal's ability to spot predators or prey approaching from above them. This is in contrast to pelagic and bentho-pelagic species that tend to possess a ventral horizontal streak (Hueter, 1980, Hueter, 1991, Bozzano and Collin, 2000), such as the tiger shark, *Galeocerdo cuvieri*, black-tipped reef shark, *Carcharinus melanopterus* (Collin, 1999) and the lemon shark, *Negaprion brevirostris* (Hueter, 1991). In pelagic species and most benthopelagic species, a ventral horizontal streak aids in predation as they scan the ocean floor below for prey (Collin and Pettigrew, 1988, Collin, 1999). The location of the visual streak in relation to a species behavioral adaptations can provide insight into its selection pressures. Although information about feeding behavior is limited, such as whether *B. waddi* ambush prey from above or scavenge for prey on the sea floors, it might be that increased resolving power is more useful in detecting

predators. *Raja bigelowi* is a benthic species with a dorsal horizontal streak, similar to *B. waddi*. Bozzano and Collin (2000) suggest that anatomical adaptations of *R. bigelowi* aid in the detection of predators as opposed to foraging for food, as this species does not ambush prey. *Brachaelurus waddi* have two nasal barbells, thus it is possible that other sensory organs, such as olfaction and electroreception, aid the localization of prey when scavenging for food on the sea floor, although it is difficult to account for without detailed information on other sensory functions in *B. waddi*.

Brachaelurus waddi has a relatively low spatial resolving power, similar to other benthic species (Collin and Pettigrew, 1988, Theiss et al., 2007, Lisney and Collin, 2008). As suggested by Hughes (1971), areas of higher cell density improve spatial resolving power and often reflect ecological relationships. For example, benthic shark species typically have low spatial resolving power, perhaps because they generally hunt slow moving prey, whereas most benthopelagic and pelagic species have higher spatial resolving power, potentially because they often prey on fast moving species like fish (Ebert et al., 2013).

4.6. Critical Flicker Fusion Frequency

Estimates of temporal resolution for *B. waddi* measured using a WNS were compared to those obtained using an SMS. Similar to the SMS method, estimates of CFFF made using the WNS increased with light intensity and there was no significant difference in the CFFF estimates between the two methods.

The WNS approach, therefore, has potential for the study of shark vision. The major benefit of this method compared to the SMS is that all frequencies of interest are presented at once, and the duration of the experiment is largely determined only by the number of replicates presented for subsequent averaging and analysis, and the number of light intensities used. Thus, the WNS method tends to be quicker to conduct, which means that rare or hard to study sharks may be studied with this technique. Based on preliminary experiments with retinal eyecup preparations conducted during this project, but not presented here, it may be possible to use the WNS method on eyes taken from recently deceased sharks, for example at fishing competitions. This may facilitate access to rare or large species (such as mako sharks, *Isurus oxyrinchus*, tiger sharks,

Galeocerdo cuvier, and great white sharks, *Carcharodon carcharias*) that cannot be studied easily in the laboratory but may provide useful data on interspecific variation in shark visual abilities.

4.7. Conclusions

This study is the first to attempt a comprehensive assessment of the visual adaptations in a benthic species. In summary, *Brachaelurus waddi* has a low temporal resolution threshold (CFFF) but is capable of functioning over a wide range of light intensities. The finding of a low temporal resolution reflects that fact that it preys on slow-moving prey and a high contrast sensitivity will be beneficial for its strongly nocturnal lifestyle. The visual pigment in the rod dominated retina appear to reflect the spectral absorption properties of the ambient light found in its typical habitat. The presence of a dorsal-horizontal visual streak reflects its benthic lifestyle and could potentially enable better spatial resolving power that may assist with prey capture or predator avoidance. This study also demonstrated that a WNS may form a useful approach for measuring temporal resolution in sharks and may facilitate access to rare tissue and broaden the understanding of interspecific variation in the visual system of sharks. This study would benefit from greater sample size and, moving forward, intends to extend the above experiments to provide a more complete characterization of the visual system of *B. waddi*.

REFERENCES

ASI, H. & PERLMAN, I. 1992. Relationships between the electroretinogram a-wave, b-wave and oscillatory potentials and their application to clinical-diagnosis. *Documenta Ophthalmologica,* 79**,** 125-139.

BATES, D., MAECHLER, M., BOKER, B. & WALKER, S. 2013. Lme4: linear mixed effects models using Eigen and S4. R package version 1. Available: http:// lme4.r-forge.r-project.org/.

BEDORE, C. N., MCCOMB, D. M., FRANK, T. F., HUETER, R. E. & KAJIURA, S. M. 2013. Effects of temperature and anesthesia on visual temporal resolution in elasmobranch fishes. *Integrative and Comparative Biology,* 53**,** E12-E12.

BOZZANO, A. 2004. Retinal specialisations in the dogfish *Centroscymnus coelolepis* from the Mediterranean deep-sea. *Scientia Marina,* 68**,** 185-195.

BOZZANO, A. & COLLIN, S. P. 2000. Retinal ganglion cell topography in elasmobranchs. *Brain Behavior and Evolution,* 55**,** 191-208.

CAO, D. C., ZELE, A. J. & POKORNY, J. 2007. Linking impulse response functions to reaction time: Rod and cone reaction time data and a computational model. *Vision Research,* 47**,** 1060-1074.

COHEN, J. H. & FRANK, T. M. 2006. Visual physiology of the Antarctic amphipod *Abyssorchomene plebs*. *Biological Bulletin,* 211**,** 140-148.

COHN, B. A., COLLIN, S. P., WAINWRIGHT, P. C. & SCHMITZ, L. 2015. *Retinal topography maps in R: New tools for the analysis and visualization of spatial retinal data*.

COIMBRA, J. P., TRÉVIA, N., MARCELIANO, M. L. V., DA SILVEIRA, A., DA COSTA, B. L., PICANÇO-DINIZ, C. W. & YAMADA, E. S. 2009. Number and distri- bution of neurons in the retinal ganglion cell layer in relation to foraging behaviors of ty- rant flycatchers. *Journal of Comparative Neurology***,** 66–73.

COLLIN, S. P. 1999. *Behavioural ecology and retinal cell topography,* Kluwer Academic Publishers, UK.

COLLIN, S. P. & PETTIGREW, J. D. 1988. Retinal topography in reef teleosts. 11. Some species with prominent horizontal streaks and high-density areae. *Brain Behavior and Evolution,* 31**,** 283-295.

CONNER, J. & MACLEOD, D. 1977. Rod photoreceptors detect rapid flicker. *Science,* 195**,** 698-699.

COREN, S. & GIRGUS, J. S. 1978. *Seeing is deceiving: the psychology of visual illusions,* Hillside (NJ), Lawrence Erlbaum Associates.

DFL. 2009. *Digital Fish Library* [Online]. University of California, San Diego: National Science Foundation. Available: http://www.digitalfishlibrary.org/library/ViewSpecies.php?id=302 [Accessed 2018].

DOWLING, J. E. & RIPPS, H. 1970. Visual adaptations in the retina of skate. *Journal of General Physiology,* 56**,** 491-520.

DUNCAN, J. 1984. Selective attention and the organisation of visual information. *Journal of Experimental Psychology General,* 113**,** 501-517.

EBERT, D. A., FOWLER, S. L. & COMPAGNO, L. J. V. 2013. *Sharks of the World,* Wild Nature Press.

FLAMARIQUE, I. N. & HAWRYSHYN, C. W. 1997. Is the use of underwater polarized light by fish restricted to crepuscular time periods? *Vision Research,* 37**,** 975-989.

FOGED, A. & POWTER, D. M. 2015. A preliminary investigation of the reproductive biology of the blind shark, *Brachaelurus waddi* (Orectolobiformes: Brachaeluridae). *Proceedings of the Linnean Society of New South Wales,* 137**,** 7-12.

FRANK, T. M. 2000. Temporal resolution in mesopelagic crustaceans. *Philosophical Transactions of the Royal Society of London Series B-Biological Sciences,* 355**,** 1195-1198.

FRITSCHES, K. A., BRILL, R. W. & WARRANT, E. J. 2005. Warm eyes provide superior vision in swordfishes. *Current Biology,* 15**,** 55-58.

GARZA-GISHOLT, E., KEMPSTER, R. M., HART, N. S. & COLLIN, S. P. 2015. Visual specializations in five sympatric species of stingrays from the family dasyatidae. *Brain Behavior and Evolution,* 85**,** 217-232.

GOVARDOVSKII, V. I., FYHRQUIST, N., REUTER, T., KUZMIN, D. G. & DONNER, K. 2000. In search of the visual pigment template. *Visual Neuroscience,* 17**,** 509-528.

GRAMONI, R. & ALI, M. A. 1970. L'électrorétinogramme et sa fréquence de fusion chez Amia calva (Linné). *Revue Canadienne De Biologie***,** 29:353–363.

GUNDERSEN, J. 1977. Notes on the estimation of the numerical density of arbitary profiles: the edge effect. *Journal of Microscopy,* 111**,** 219-23.

HARAHUSH, B. K., HART, N. S., GREEN, K. & COLLIN, S. P. 2009. Retinal neurogenesis and ontogenetic changes in the visual system of the brown banded bamboo shark, *Chiloscyllium punctatum (Hemiscyllidae, Elasmobranchii)*. *Journal of Comparative Neurology,* 513**,** 83-97.

HART, N. S. 2002. Vision in the peafowl (*Aves : Pavo cristatus)*. *Journal of Experimental Biology,* 205**,** 3925-3935.

HART, N. S. 2004. Microspectrophotometry of visual pigments and oil droplets in a marine bird, the wedge-tailed shearwater *Puffinus pacificus*: topographic variations in photoreceptor spectral characteristics. *Journal of Experimental Biology,* 207**,** 1229-1240.

HART, N. S., LISNEY, T. J. & COLLIN, S. P. 2006. Visual communication in elasmobranchs. *Communication in Fishes***,** 56.

HART, N. S., LISNEY, T. J., MARSHALL, N. J. & COLLIN, S. P. 2004. Multiple cone visual pigments and the potential for trichromatic colour vision in two species of elasmobranch. *Journal of Experimental Biology,* 207**,** 4587-4594.

HART, N. S., PARTRIDGE, J. C. & CUTHILL, I. C. 1998. Visual pigments, oil droplets and cone photoreceptor distribution in the European starling (*Sturnus vulgaris)*. *Journal of Experimental Biology,* 201**,** 1433-1446.

HART, N. S., THEISS, S. M., HARAHUSH, B. K. & COLLIN, S. P. 2011. Microspectrophotometric evidence for cone monochromacy in sharks. *Naturwissenschaften,* 98**,** 193-201.

HEMMI, J. M., JAMES, A. & TAYLOR, W. 2002. Color opponent retinal ganglion cells in the tammar wallaby retina. *Journal of Vision,* 2.

HUETER, R. E. 1980. *Physiological optics of the eye of the juvenile lemon shark (Negaprion brevirostris).* M.Sc. Thesis, University of Miami.

HUETER, R. E. 1991. Adaptations for Spatial Vision in Sharks. *Journal of Experimental Zoology,* 5**,** 130-141.

HUGHES, A. 1971. Topographical relationships between the anatomy and physiology of the rabbit visual system. *Documenta Ophthalmologica,* 30**,** 33–159.

IKEDA, H. & WRIGHT, M. 1972. Receptive field organization of 'sustained'and 'transient'retinal ganglion cells which

subserve different functional roles. *Journal of Physiology,* 227**,** 769-800.

INFANTOSI, A. F. C., MELGES, D. B. & TIERRA-CRIOLLO, C. J. 2006. Use of magnitude-squared coherence to identify the maximum driving response band of the somatosensory evoked potential. *Brazilian Journal of Medical and Biological Research***,** 1593-1603.

KALINOSKI, M., HIRONS, A., HORODYSKY, A. & BRILL, R. 2014. Spectral sensitivity, luminous sensitivity, and temporal resolution of the visual systems in three sympatric temperate coastal shark species. *Journal of Comparative Physiology a-Neuroethology Sensory Neural and Behavioral Physiology,* 200**,** 997-1013.

KELLEY, L. A. & KELLEY, J. L. 2014. Animal visual illusion and confusion: the importance of a perceptual perspective. *Behavioral Ecology,* 25**,** 450-463.

LAND, M. F. & NILSSON, D. E. 2012. *Animal Eyes,* United Kingdom, Oxford University.

LAST, P. R. & STEVENS, J. D. 1994. *Sharks and Rays of Australia,* CSIRO Australia.

LEVINE, J. S. & MACNICHOL, E. F., JR. 1985. *Microspectrophotometry of primate photoreceptors: art, artifact, and analysis,* Liss, New York.

LISNEY, T. J. & COLLIN, S. P. 2008. Retinal ganglion cell distribution and spatial resolving power in elasmobranchs. *Brain, Behavior and Evolution,* 72**,** 59-77.

LISNEY, T. J., THEISS, S. M., COLLIN, S. P. & HART, N. S. 2012. Vision in elasmobranchs and their relatives: 21st century advances. *Journal of Fish Biology,* 80**,** 2024-2054.

LITHERLAND, L. & COLLIN, S. P. 2008. Comparative visual function in elasmobranchs: Spatial arrangement and ecological correlates of photoreceptor and ganglion cell distributions. *Visual Neuroscience,* 25**,** 549-561.

LOEW, E. R. & LYTHGOE, J. N. 1978. The ecology of cone pigments in teleost fishes. *Vision Research,* 18**,** 715-22.

LYTHGOE, J. N. 1980. Vision in fishes: ecological adaptations. *Environmental physiology of fishes,* 35**,** 431-445.

MALMSTROM, T. & KROGER, R. H. 2006. Pupil shapes and lens optics in the eyes of terrestrial vertebrates. *Journal of Experimental Biology,* 209**,** 18-25.

MARMARELIS, P. Z. & MARMARELIS, V. Z. 1978. *Analysis of Physiological Systems, The White-Noise Approach,* New York, Plenum Press.

MATTHIESSEN, L. 1880. Untersuchungen über den Aplanatismus und die Periscopie der Krystalllinsen in den Augen der Fische. *Pflügers Arch Eur Journal of Physiology,* 21**,** 287–307.

MCCOMB, D. M., FRANK, T. M., HUETER, R. E. & KAJIURA, S. M. 2010. Temporal resolution and spectral sensitivity of the visual system of three coastal shark species from different light environments. *Physiological and Biochemical Zoology,* 83**,** 299-307.

MCCOMB, D. M., TRICAS, T. C. & KAJIURA, S. M. 2009. Enhanced visual fields in hammerhead sharks. *Journal of Experimental Biology,* 212**,** 4010-4018.

MCFARLAND, W. 1990. Light in the sea: the optical world of elasmobranchs. *Journal of Experimental Zoology,* 256(suppl.S5)**,** 3-12.

MCFARLAND, W. & LOEW, E. R. 1883. Wave produced changes in underwater light and their relations to vision. *Environmental Biology of Fishes,* 8**,** 173-184.

MCFARLAND, W. N. 1986. Light in the sea- correlations with behaviors of fishes and invertebrates. *American Zoologist,* 26**,** 389-401.

MUSTONEN, J., ROVAMO, J. & NASANEN, R. 1993. The effects of grating area and spatial frequency on contrast sensitivity as a function of light level. *Vision Research,* 33**,** 2065-2072.

PAULSSON, L. & SJOSTRAND, J. 1980. Contrast sensitivity in the presence of glare light. *Investigative Ophthalmology & Visual Science,* 19**,** 401-406.

PEPPERBERG, D. R., BROWN, P. K., LURIE, M. & DOWLING, J. E. 1978. Visual pigment and photoreceptor sensitivity in the isolated skate retina. *The Journal of General Physiology,* 71**,** 369-396.

RABINER, L. R. & GOLD, B. 1975. *Theory and Application of Digital Signal Processing,* Englewood Cliffs, NJ, Prentice-Hall.

RYAN, L. A., HART, N. S., COLLIN, S. P. & HEMMI, J. M. 2016. Visual resolution and contrast sensitivity in two benthic sharks. *Journal of Experimental Biology,* 219**,** 3971-3980.

RYAN, L. A., HEMMI, J. M., COLLIN, S. P. & HART, N. S. 2017. Electrophysiological measures of temporal resolution, contrast sensitivity and spatial resolving power in sharks. *Journal of Comparative Physiology a-Neuroethology Sensory Neural and Behavioral Physiology,* 203**,** 197-210.

RYAN, L. A., MEEUWIG, J. J., HEMMI, J. M., COLLIN, S. P. & HART, N. S. 2015. It is not just size that matters: shark cruising speeds are species-specific. *Marine Biology,* 162**,** 1307-1318.

SCHIEBER, N. L., COLLIN, S. P. & HART, N. S. 2012. Comparative retinal anatomy in four species of elasmobranch. *Journal of Morphology,* 273**,** 423-440.

SHAND, J., HART, N. S., THOMAS, N. & PARTRIDGE, J. C. 2002. Developmental changes in the cone visual pigments of black bream *Acanthopagrus butcheri*. *Journal of Experimental Biology,* 205**,** 3661-3667.

STEINBERG, R. H., SCHMIDT, R. & BROWN, K. T. 1970. Intracellular Responses to Light from Cat Pigment Epithelium: Origin of the Electroretinogram c-Wave. *Nature,* 227**,** 728.

STERRATT, D. C., LYNGHOLM, D., WILLSHAW, D. J. & THOMPSON, I. D. 2013. Standard anatomical and visual space for the mouse retina: computational reconstruction and transformation of flattened retinae with the retistruct package. *PLOS Computational Biology,* 9**,** 2.

THEISS, S. M., DAVIES, W. I. L., COLLIN, S. P., HUNT, D. M. & HART, N. S. 2012. Cone monochromacy and visual pigment spectral tuning in wobbegong sharks. *Biology Letters,* 8**,** 1019-1022.

THEISS, S. M., LISNEY, T. J., COLLIN, S. P. & HART, N. S. 2007. Colour vision and visual ecology of the blue-spotted maskray, *Dasyatis kuhlii* Muller & Henle, 1814. *Journal of Comparative Physiology a-Neuroethology Sensory Neural and Behavioral Physiology,* 193**,** 67-79.

ULLMANN, J. F. P., MOORE, B. A., TEMPLE, S. E., FERNANDEZ-JURICIC, E. & COLLIN, S. P. 2012. The retinal wholemount technique: A window to understanding the brain and behaviour. *Brain Behavior and Evolution,* 79**,** 26-44.

WALLS, G. 1942. *The Vertebrate Eye and Its Adaptive Radiation,* Hafner, New York.

WANDELL, B. A. 1996. *Foundations of vision,* Sunderland, MA, Sinauer Associates Inc.

WARRANT, E. J. 1999. Seeing better at night: life style, eye design and the optimum strategy of spatial and temporal summation. *Vision Research,* 39**,** 1611-1630.

WARRANT, E. J. & JOHNSEN, S. 2013. Vision and the light environment. *Current Biology,* 23**,** R990-R994.

WARRANT, E. J. & LOCKET, N. A. 2004. Vision in the deep sea. *Biological Reviews,* 79**,** 671-712.

WARRINGTON, R. E., HART, N. S., POTTER, I. C., COLLIN, S. P. & HEMMI, J. M. 2017. Retinal temporal resolution and contrast sensitivity in the parasitic lamprey *Mordacia mordax* and its non-parasitic derivative *Mordacia praecox*. *Journal of Experimental Biology,* 220**,** 1245-1255.

WELCH, P. D. 1967. The use of Fast Fourier Tranform for the estimation of power spectra: A method based on time averaging over short, modified periodograms. *Ieee Transactions on Image Processing,* 15**,** 70-73.

YEW, D. T., CHAN, Y. W., LEE, M. & LAM, S. 1984. A biophysical, morphological and morphometric survey of the eye of the small shark *(Hemiscyllium plagiosum)*. *Anatomischer Anzeiger,* 155**,** 355-363.

ZAR, J. H. 1999. *Biostatistical analysis,* Prentice-Hall, US.

ZELE, A. J., FEIGL, B., KAMBHAMPATI, P. K., AHER, A., MCKEEFRY, D., PARRY, N., MAGUIRE, J., MURRAY, I. & KREMERS, J. 2017. A temporal white noise analysis for extracting the impulse response function of the human electroretinogram. *Translational Vision Science & Technology,* 6.

Appendix A.

In this study, we developed and validated the WNS technique in two other model species, the epaulette shark, *Hemscyllium ocellatum*, and five Australian Bull Ants, *Myrmecia midas*. Figures represent the temporal thresholds at four light intensities (ND 3.5, 2, 1, 0) for both WNS (black) and SMS (red).

Hemiscyllium ocellatum, epaulette Shark

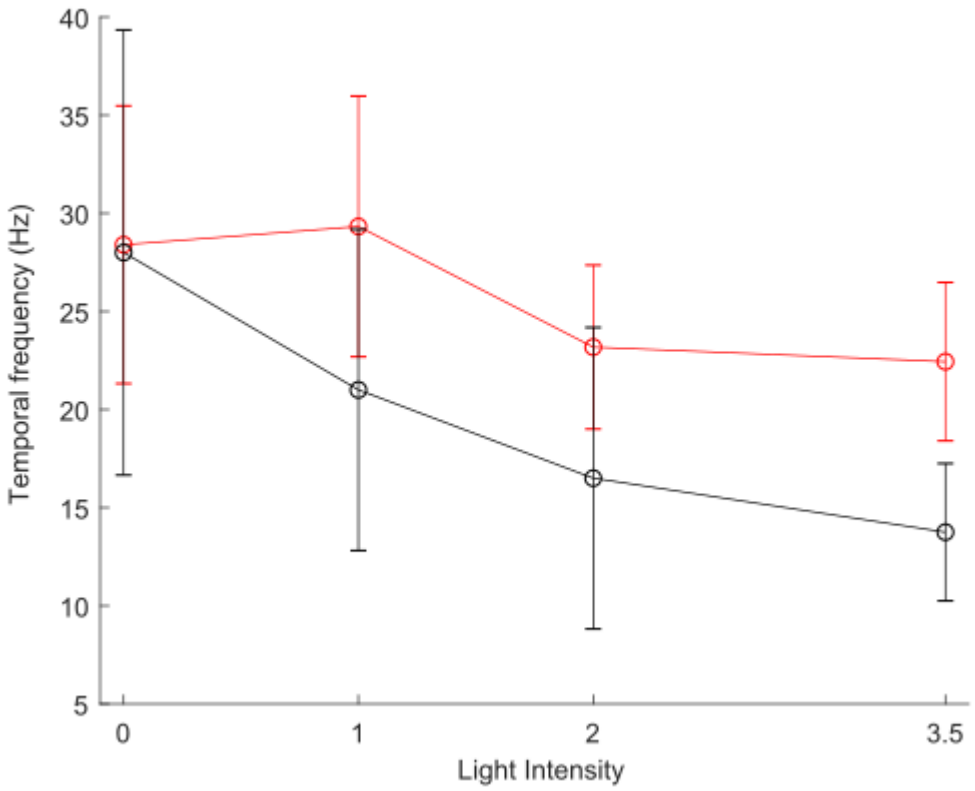

Figure 1: Estimated critical flicker fusion frequencies (CFFF) at 4 different light intensities for one individual *Hemiscyllium ocellatum* over four separate experiments using a white noise stimulus (WNS; black open circle represent species mean and bars show +/- 1 std. dev) and sinusoidally modulated stimulus (SMS; red, open circle represent species mean and bars show +/- 1 std. dev).

Myrmecia midas, Australian Bull Ant

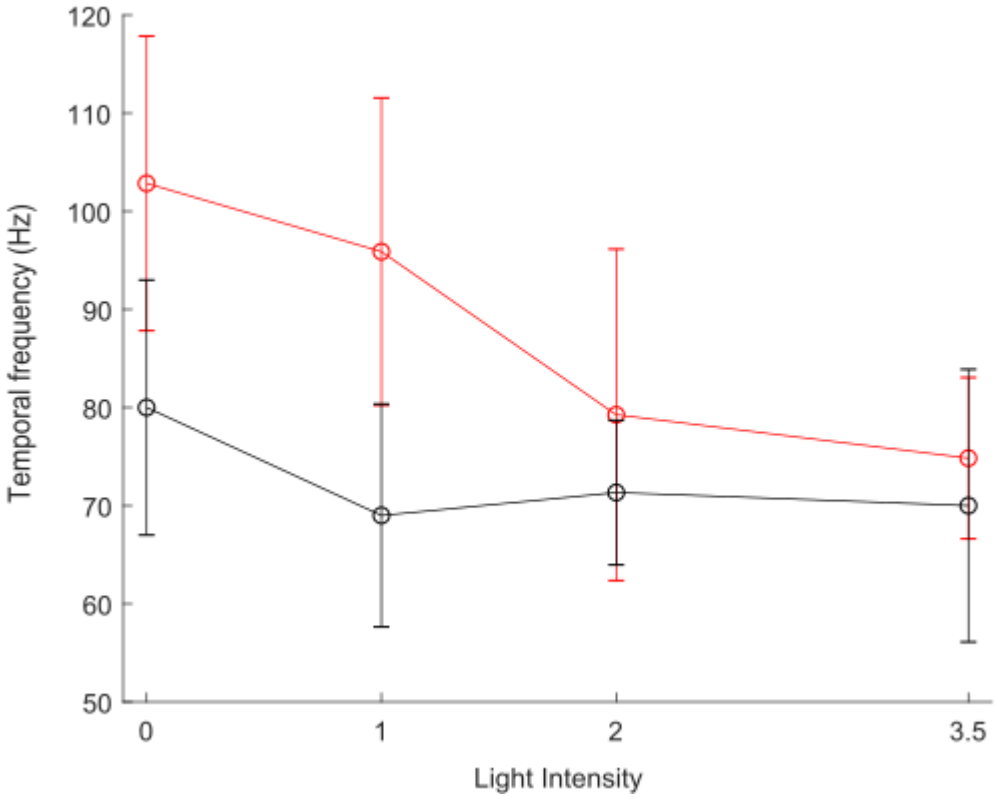

Figure 2: Estimated critical flicker fusion frequencies (CFFF) at 4 different light intensities for *Myrmecia midas* (n=4) using a white noise stimulus (WNS; black open circle represent species mean and bars show +/- 1 std. dev) and sinusoidally modulated stimulus (SMS; red, open circle represent species mean and bars show +/- 1 std. dev).